



**HAL**  
open science

## **ASC-1 Is a Cell Cycle Regulator Associated with Severe and Mild Forms of Myopathy**

Rocío Villar-quiles, Fabio Catervi, Eva Cabet, Raul Juntas-Morales, Casie A Genetti, Teresa Gidaro, Asuman Koparir, Adnan Yüksel, Sandra Coppens, Nicolas Deconinck, et al.

► **To cite this version:**

Rocío Villar-quiles, Fabio Catervi, Eva Cabet, Raul Juntas-Morales, Casie A Genetti, et al.. ASC-1 Is a Cell Cycle Regulator Associated with Severe and Mild Forms of Myopathy. *Annals of Neurology*, 2020, 87 (2), pp.217-232. 10.1002/ana.25660 . hal-02957769

**HAL Id: hal-02957769**

**<https://hal.science/hal-02957769>**

Submitted on 5 Oct 2020

**HAL** is a multi-disciplinary open access archive for the deposit and dissemination of scientific research documents, whether they are published or not. The documents may come from teaching and research institutions in France or abroad, or from public or private research centers.

L'archive ouverte pluridisciplinaire **HAL**, est destinée au dépôt et à la diffusion de documents scientifiques de niveau recherche, publiés ou non, émanant des établissements d'enseignement et de recherche français ou étrangers, des laboratoires publics ou privés.

**ASC1 is a cell cycle regulator associated with severe and mild forms of myopathy**

Running title: ASC1-related myopathy phenotype &amp; pathophysiology

Rocío N Villar-Quiles, MD<sup>1,2</sup>, Fabio Catervi, MS<sup>1</sup>, Eva Cabet, PhD<sup>1</sup>, Raul Juntas-Morales, MD<sup>3</sup>, Casie A. Genetti, MS<sup>4</sup>, Teresa Gidaro, MD, PhD<sup>5</sup>, Asuman Koparir, MD<sup>6</sup>, Adnan Yüksel, MD<sup>6</sup>, Sandra Coppens, MD<sup>7</sup>, Nicolas Deconinck, MD, PhD<sup>7</sup>, Emma Pierce-Hoffman, BSc<sup>8</sup>, Xavière Lornage, PhD<sup>9</sup>, Julien Durigneux<sup>10</sup>, Jocelyn Laporte, PhD<sup>9</sup>, John Rendu, PharmD, PhD<sup>11</sup>, Norma B. Romero, MD, PhD<sup>2,12</sup>, Alan H. Beggs, MD, PhD<sup>4</sup>, Laurent Servais, MD, PhD<sup>5,13</sup>, Mireille Cossée, MD<sup>14</sup>, Montse Olivé, MD, PhD<sup>15</sup>, Johann Böhm, PhD<sup>9</sup>, Isabelle Duband-Goulet, PhD<sup>1\*#</sup>, Ana Ferreira, MD, PhD<sup>1,2\*#</sup>

\* last co-authors with equal contribution as senior authors

# joint corresponding authors

<sup>1</sup>Basic and Translational Myology Laboratory, UMR8251, Université de Paris/CNRS, Paris, France

<sup>2</sup>Reference Center for Neuromuscular Disorders, Pitié-Salpêtrière Hospital, AP-HP, Institute of Myology, Paris, France

<sup>3</sup>Neuromuscular Unit, CHU Montpellier/EA7402 Université de Montpellier, IURC, Institut Universitaire de Recherche Clinique, Montpellier, France

<sup>4</sup>The Manton Center for Orphan Disease Research, Division of Genetics and Genomics, Boston Children's Hospital, Harvard Medical School, Boston, MA 02115, USA

<sup>5</sup>I-Motion, Institute of Myology AP-HP, Paris, France

<sup>6</sup>Biruni University, Department of Molecular Biology and Genetics, Istanbul, Turkey

<sup>7</sup>Department of Paediatric Neurology, Reference Neuromuscular Center, Hôpital Universitaire des Enfants Reine Fabiola HUDERF, Université Libre de Bruxelles, ULB, Brussels, Belgium

<sup>8</sup>Center for Mendelian Genomics, The Broad Institute of MIT and Harvard, Cambridge, MA 02142, USA

<sup>9</sup>Department of Translational Medicine and Neurogenetics, IGBMC (Institut de Génétique et de Biologie Moléculaire et Cellulaire), Inserm U1258, CNRS UMR7104, Université de Strasbourg, Illkirch, France

<sup>10</sup>Centre de référence des maladies neuromusculaires AOC, Service de Neuropédiatrie, CHU Angers, France

<sup>11</sup>Laboratoire de Biochimie et Génétique Moléculaire, CHU Grenoble, France

<sup>12</sup>Neuromuscular Morphology Unit, Institute of Myology, Pitié-Salpêtrière Hospital, Paris, France

<sup>13</sup>Division of Child Neurology, Centre de Référence des Maladies Neuromusculaires, Department of Pediatrics, University Hospital Liège & University of Liège, Belgium

<sup>14</sup>Molecular Genetics Laboratory, CHU Montpellier/INSERM U827, Institut Universitaire de Recherche Clinique, Montpellier, France

<sup>15</sup>Neuropathology Unit, Department of Pathology and Neuromuscular Unit, IDIBELL-Hospital Universitari de Bellvitge, Barcelona, Spain

Corresponding authors:

Isabelle Duband-Goulet and Ana Ferreiro

Basic & Translational Myology Laboratory

Unité de Biologie Fonctionnelle et Adaptative

Université Paris Diderot – CNRS

35, rue Hélène Brion

75205 Paris cedex 13, France

Tel: (33) (0)1 57 27 79 65

E-mail : [isabelle.duband-goulet@univ-paris-diderot.fr](mailto:isabelle.duband-goulet@univ-paris-diderot.fr); ana.b.ferreiro@gmail.com

Number of characters in the title: 80

Number of characters in the running head: 49

Number of words in the abstract: 250

Number of words in the Introduction: 501

Number of words in the Discussion: 1535

Number of words in the body of the manuscript: 4485

Number of figures:6

Number of color figures: 4 (Figures 2,3,4,5)

Number of tables: 2

## **ABSTRACT**

### Objective

Recently, the ASC-1 complex has been identified as a mechanistic link between ALS and spinal muscular atrophy (SMA), and three mutations of the ASC-1 gene *TRIP4* have been associated with SMA or congenital myopathy. Our goal was to define ASC-1 neuromuscular function and the phenotypical spectrum associated with *TRIP4* mutations.

### Methods

Clinical, molecular, histological and MRI studies in 5 families with 7 novel *TRIP4* mutations. FACS and Western blot in patient-derived fibroblasts and muscles and in *Trip4* knocked-down C2C12 cells.

## Results

All mutations caused ASC-1 protein depletion. The clinical phenotype was purely myopathic, ranging from lethal neonatal to mild ambulatory adult patients. It included early-onset axial and proximal weakness, scoliosis, rigid spine, dysmorphic facies, cutaneous involvement, respiratory failure and, in the older cases, dilated cardiomyopathy. Muscle biopsies showed multiminicores, nemaline rods, cytoplasmic bodies, caps, central nuclei, rimmed fibers and/or mild endomysial fibrosis. ASC-1 depletion in C2C12 and in patient-derived fibroblasts and muscles caused accelerated proliferation, altered expression of cell cycle proteins and/or shortening of the G0/G1 cell cycle phase leading to cell size reduction.

## Interpretation

Our results expand the phenotypical and molecular spectrum of *TRIP4*-associated disease to include mild adult forms with or without cardiomyopathy, associate ASC-1 depletion with primary pure muscle involvement and establish *TRIP4* as a causative gene for several congenital muscle diseases including nemaline, core, centronuclear or cytoplasmic-body myopathies. They also identify ASC-1 as a novel cell cycle regulator with a key role in cell proliferation, and underline transcriptional co-regulation defects as a novel pathophysiological mechanism.

## INTRODUCTION

Congenital myopathies (CMs) are genetically and clinically heterogeneous inherited disorders. They usually present during the first years of life with delayed motor development, muscular weakness and hypotonia and have a stable or slowly progressive course. CMs are sometimes associated with cardiac and/or respiratory failure<sup>1-3</sup> and have no specific treatment<sup>4</sup>. More than 20 genes have been associated with CMs<sup>5,6</sup>, most of them encoding proteins involved in (i) skeletal muscle calcium homeostasis<sup>7</sup>; (ii) excitation-contraction coupling<sup>8</sup>; (iii) membrane remodeling<sup>9,10</sup> and (iv) myofibrillar force generation<sup>11</sup> or thin-thick filament assembly<sup>12</sup> and interactions<sup>13</sup>. However, the genetic defect remains unknown in

up to 25% CM patients.

In 2016, we described a form of congenital myopathy caused by recessive mutations in Thyroid Hormone Receptor Interactor 4 (*TRIP4*), encoding the transcriptional coactivator ASC-1 (Activating Signal Cointegrator-1), in a large consanguineous family. ASC-1 defines the ASC-1 transcriptional cointegrator complex, together with three other subunits (ASCC1, ASCC2 and ASCC3). We termed this novel condition ASC-1 Related Myopathy (ASC1-RM), thus identifying transcriptional coregulation as a novel CM pathomechanism<sup>14</sup>. Patients presented with severe neonatal hypotonia, potentially-lethal respiratory failure, muscle weakness with partial or no ambulation, scoliosis, joint hyperlaxity and skin abnormalities. Muscle biopsy revealed the so-far unreported association of multimimicres, caps and dystrophic lesions.

The role of the ASC-1 complex in neuromuscular diseases was confirmed by the simultaneous description of recessive mutations in *TRIP4* (three families sharing two mutations) or in *ASCC1* (one family)<sup>15</sup> in patients diagnosed with Spinal Muscular Atrophy (SMA) with arthrogryposis multiplex congenita, respiratory distress and congenital bone fractures. Thereafter, no other patient with *TRIP4* mutations has been described, but four additional families with *ASCC1* recessive nonsense or frameshift mutations have been recently reported<sup>16,17</sup>. They showed a similar neonatal phenotype including arthrogryposis, bone fractures and respiratory failure, but muscle biopsies disclosed myopathic features and were not suggestive of motoneuron involvement<sup>17</sup>.

Transcriptional co-regulators are emerging as key modulators of the functions of nuclear receptors and transcription factors<sup>18</sup>. The ASC-1 complex acts as a coactivator through direct binding to transcription factors like AP-1, NF-kappa-B and Serum Response Factor (SRF), involved in cell fate-controlling pathways<sup>19</sup>. ASC-1 is known to interact with basal transcription factors (TBP, TFIIA), transcription integrators (CBP, SRC-1) and nuclear receptors (TR, RXR, ER) *in vitro* through its highly conserved zinc finger domain<sup>20</sup>. Moreover, ASC-1 contains a conserved C-terminal ASCH domain with putative RNA-binding activity predicted *in silico* to coordinate pre-mRNA processing<sup>21,22</sup>. Interestingly, the ASC-1 complex has been recently implicated in Amyotrophic Lateral Sclerosis (ALS) pathogenesis,

being proposed as a common link between ALS and SMA<sup>23</sup>. We demonstrated that ASC-1 plays a pivotal role in muscle, its absence leading to defects in human myotube growth<sup>14</sup>. However, the precise ASC-1 function and the phenotypical spectrum associated with *TRIP4* mutations (including motoneuron versus primary muscle involvement) remained largely unknown.

We report here the first series of patients with *TRIP4* mutations, redefine the phenotypical and molecular spectrum of disease and establish the first phenotype-genotype correlations. We also clarify the disease pathophysiology by revealing an unsuspected function of ASC-1 as a cell cycle regulator.

## **METHODS**

### **Patients and biological samples**

Patients were recruited through an international collaboration. We also reassessed evolution of the previously-reported ASC1-RM family<sup>14</sup>. Clinical data were systematically retrieved and analyzed retrospectively according to a standardized form. All patients were examined by at least one of the authors in specialized neuromuscular departments.

Diagnostic muscle biopsies from four patients were processed for standard histological and immunochemical studies and fixed for electron microscopy. Primary fibroblasts from patients and age-paired controls were obtained from skin biopsies or surgically-discarded tissues. Muscle tissue was obtained from diagnostic biopsies in two patients and from surgically-discarded tissue in controls.

Informed consent was obtained from all patients or their guardians in agreement with local Ethic Committees and with the 1964 Helsinki declaration and its later amendments.

### **Genotyping**

*TRIP4* mutations were identified on DNA from peripheral blood samples by exome sequencing or next-generation sequencing-based myopathy genes panel, Sanger-confirmed in patients and relatives

and reported according to Human Genome Variation Society recommendations (<http://varnomen.hgvs.org>).

Exome Aggregation Consortium (ExAC, <http://exac.broadinstitute.org/>) and Genome Aggregation (gnomAD, <http://gnomad.broadinstitute.org/>) databases were interrogated to identify previously-reported mutations and to determine the frequency of each mutation in the general population. Alamut® Visual (Interactive Biosoftware, North Seattle, WA) was used to predict the effect of the variants.

### **Cell Culture**

All cells were grown at 37°C with 5% CO<sub>2</sub>. Cells were grown in Dulbecco Modified Eagle Media containing Glutamax (Gibco), fetal calf serum (FCS) 20% and penicillin-streptomycin (P/S) 1% (primary fibroblasts) or FCS 10% and P/S 1% (C2C12).

### **Transfection: siRNA and Plasmid DNA**

C2C12 were transfected with *Trip4*-specific siRNAs or scrambled control siRNA (Origene) 18 hours after seeding according to the manufacturer's instructions using Lipofectamine RNAimax (Invitrogen). The final concentration of siRNAs was 4 nM. Maximum down-regulation was achieved 48h post transfection.

For rescue experiments, mammalian expression vectors (Promega) containing the ORF sequence of the human *TRIP4* (pFN21AB7885) or *CELF1* (pFN21AB0039) genes fused with a HaloTag were used. Cells were transfected with siRNAs as described above. A second transfection was performed to overexpress *TRIP4* or *CELF*. Plasmids and Lipofectamine 2000 were mixed in Opti-MEM according to the manufacturer's instructions (Invitrogen).

### **Cell proliferation studies**

After seeding at 40000cells/well, the number of primary fibroblasts per optical field was counted from 24 to 96 hours on bright-field images. Proliferation of C2C12 cells was analyzed from 24 to 72 hours after transfection.

### **Cell size measurements**

C2C12 were imaged from 24 to 96h post-seeding on a Zeiss Axio Observer A1 inverted microscope. Length and width of cells were measured on bright-field images with Image J (National Institute of Health, Bethesda, MS, USA).

### **Fluorescence Activated Cell Sorting (FACS) Analysis**

C2C12 were harvested 48 hours after transfection and primary fibroblasts during exponential growth phase. Cells were fixed in 70% ethanol at -20°C overnight and then stained with 50µg/ml of propidium iodide, 0.1 or 1% triton and 100 or 50 µg/ml RNase A for fibroblasts or C2C12 respectively. Analysis was performed using Cyan-ADP analyser and FlowJo-software.

### **Population doubling time and cell phase duration**

Doubling time was calculated using the website [doubling-time.com/compute.php](http://doubling-time.com/compute.php) (Roth, A., 2006, Doubling time computing) and the formula

$$\text{Doubling Time} = \frac{\text{duration} \log(10)}{\log(\text{Final Concentration}) - \log(\text{Initial Concentration})}$$

The duration of each cell phase was obtained by multiplying each sample doubling time by the percentage of cells in each phase (FACS).

### **Western Blot**

Cells were lysed with cold lysis buffer. Cell extracts (20 µg) were separated using 10% SDS-PAGE gel and transferred on nitrocellulose membranes (Bio-Rad Trans Turbo Transfer system) which were blocked and probed with the primary antibodies anti-ASC-1 (Abcam), anti-tubulin (Sigma), anti-p21 (Santa-Cruz), anti-cyclin D3 (Santa-Cruz), anti-cyclin D1 (Santa-Cruz or Millipore), anti-pRb (BD Pharmingen), anti-MHCe (DSHB) or anti-halotag (Promega). Membranes were incubated with the secondary antibodies goat anti-rabbit HRP conjugate (Thermo Scientific) or goat anti-mouse HRP

conjugate (Thermo Scientific). Signals were detected with Enhanced chemiluminescence (ECL, Bio-Rad) and quantified using Image J software.

### **Statistical analyses**

Results were expressed as mean  $\pm$  standard deviation. All data were analyzed with the SPSS® Statistics version 22.0 (Armonk, NY: IBM Corp.). Differences were considered significant if p-value was  $<0.05$ .

## **RESULTS**

### **Clinical findings: Expanding the clinical spectrum**

We identified six novel patients (two females and four males) from five families with *TRIP4* mutations (Table 1). Age at ascertainment ranged from 7 to 63 years. All pedigrees were compatible with autosomal recessive transmission. Consanguinity was confirmed in three families (A, C and E). Patient CIII.7 had two siblings deceased during the first year of life due to respiratory distress. Patient DII.2 had a brother diagnosed with a congenital myopathy with type I fiber uniformity who died at 5 years due to respiratory failure. These three affected siblings were not included due to lack of genetic confirmation. We also reassessed the three surviving patients from the originally reported family (family F<sup>14</sup>) after three years of additional follow-up.

Overall, the clinical phenotype in the novel patients was marked, like in the original family, by early onset proximal and axial weakness, respiratory failure with variable severity, scoliosis and skin involvement without prominent limb contractures.

None of the patients presented with arthrogryposis or congenital contractures. There were no complications during pregnancy or labor, excepting reduced fetal movements in the most severe patient (CIII.7). First signs appeared before adulthood in all cases.

Patient CIII.7 presented at birth with severe neonatal hypotonia, poor antigravity limb movements, dysmorphic features, feeding difficulties, perinatal asphyxia and respiratory distress (Fig. 1A). He never acquired cephalic control. Two patients (AIII.2 and DII.2) presented with neonatal hypotonia and delayed motor milestones. The two siblings from family B presented with delayed gait acquisition, waddling gait and fatigability. The mildest patient (EII.4) presented with difficulties for running and poor sports performance in adolescence. The last five patients acquired independent ambulation, although only one did so before the age of 18 months.

In all patients from the six families, muscle weakness and amyotrophy was predominantly axial and proximal (3-4/5, Medical Research Council scale), while distal limb strength was relatively well preserved. Only one patient had marked facial weakness. There was bilateral horizontal ophthalmoparesis in one patient and ophthalmoplegia in the most severe case. Ptosis was not observed.

Muscle weakness was stable or slowly progressive. Excepting the three patients from the original family F, who never acquired independent ambulation, all the adult patients can walk outdoors without support at ages 23-63 years, walking distance being limited by fatigue or dyspnea. Three patients are able to climb stairs with aid. Patient AIII.2, currently 9 years old, is still improving her motor abilities and starting to run.

All the patients who survived beyond childhood, except the mildest patient EII.4, had early-onset progressive scoliosis, associated with lateral trunk deviation and tilted pelvis in two cases (Fig. 1A). This includes the youngest patient of family F (FIII.1), reassessed after arthrodesis at age 12 years. Scoliosis was associated with spinal rigidity in a total of five cases. Thorax deformities (flat thorax and pectus excavatum) were present in five patients. Five also had dysmorphic craniofacial features with a similar flat face, along with a large and thick neck appearance.

Respiratory failure was present in 9 of the 10 patients since childhood. The most severe patient suffered neonatal respiratory distress requiring tracheostomy and assisted ventilation. He died at 8 months due to respiratory failure, and so did patient FII.5 at 16 months. Five patients needed chronic ventilation (nocturnal non-invasive in three cases, through a tracheostomy in two), while in the

remaining two cases only respiratory physiotherapy was prescribed. The mildest patient, currently aged 63, has a FVC of 80% but is treated with CPAP due to sleep apnea/hypopnea syndrome.

No patient had congenital or childhood cardiomyopathy. However, patient EII.4 developed a severe dilated cardiomyopathy (DCM) in the fifth decade, requiring a preventive automated implantable cardioverter defibrillator. Follow-up of family F revealed DCM from the beginning of the third decade in patient FII.2. All the other patients have normal cardiac evaluations at ages 9-35 years.

Limb contractures, mild to moderate, were present in five patients, mainly affecting Achilles tendon and elbows. Prominent and generalized joint hyperlaxity was observed in five. Deep tendon reflexes were universally diminished or absent.

Extramuscular involvement included skin abnormalities (hyperelasticity, follicular hyperkeratosis, and xerosis with scratch lesions but without keloids, N=7) and body composition changes. Three of the novel patients were underweight (<4<sup>th</sup> percentile) and one was overweight with abundant adipose tissue in lower limbs, resembling the female patients from family F<sup>14</sup>. None of the novel patients had intellectual disability or signs of CNS abnormalities.

CK level was normal or mildly elevated (<3xN) in all patients. Electromyography showed a myopathic pattern without denervation or abnormalities in nerve conduction studies (N=6) or repetitive stimulation (N=3).

Muscle MRI of the lower limbs in two of the novel patients showed a predominant involvement of the posterior compartment of the thigh, notably of gluteus maximus and adductor longus muscles with relative preservation of gracilis, sartorius, and semitendinosus muscles (Fig. 1B). This pattern was comparable to that previously observed in family F<sup>14</sup>.

### **Histopathological phenotype: cores, cytoplasmic bodies, nemaline, centronuclear, and cap lesions**

One patient had a quadriceps biopsy in early childhood, reportedly normal, which was not available. Samples from the remaining four biopsied patients showed congenital myopathy lesions, including

fiber size variability, type 1 fiber predominance (and frequent hypertrophy) and internalized nuclei, along with other changes in the muscle fiber architecture (Table 2, Fig.2). Three patients had multi-minicores, often associated with other forms of sarcomere disorganization (cap lesions, rods and cytoplasmic bodies, whorled fibers). The most severe patient showed fibers with centrally located nuclei interspersed with very small, rounded fibers without fascicular distribution, compatible with centronuclear/myotubular myopathy.

Lobulated fibers and rimmed sarcolemma (intense oxidative rims beneath the sarcolemma, Fig. 2e) were -occasionally observed. None of the four biopsies disclosed fiber type grouping, angulated fibers or group atrophy suggestive of denervation.

#### **Genetic studies: Novel *TRIP4* mutations**

Seven previously unreported mutations in the *TRIP4* gene were identified (Fig. 3A-B). Transmission was autosomal recessive in all cases. Tested parents from three families were healthy heterozygous carriers.

The mutations were distributed along the entire length of the gene. These included the first *TRIP4* missense variant, affecting a highly-conserved residue in the Zinc finger domain (c.534C>G, p. His178Gln). Two frameshift mutations predicted loss of the ASCH domain (c.1544\_1547delACTG, p.Asp515Alafs\*34 and homozygous deletion of exons 8 and 9, respectively) (Fig. 3C).

Western blot was performed on primary skin fibroblast cultures (family B) or frozen muscle biopsies (family D and E) from four patients. Family B was compound heterozygous for a missense and a truncating mutation, which led to a reduced level of expression of the full-length protein (10-20% compared to control) (Fig. 3D). Frameshift mutations (family D) or large deletions affecting the C-terminal part of the protein (family E) led to a total absence of full length ASC-1 and no detectable truncated form (Fig. 3E).

None of the patients had mutations in other known neuromuscular genes except for the oldest patient (EII.4), in which exome studies revealed a heterozygous variant of the titin gene (*TTN*)

(c.6379\_6380del, p.Tyr2127Leufs\*8), also identified in one of his asymptomatic older sisters whose echocardiography was normal. This variant, predicted to lead to a truncated protein, was absent from ExAC and was not associated with any other *TTN* change (including missense variants) in the patient.

### **ASC-1 defects alter proliferation of patient fibroblasts and myogenic cells**

When amplifying primary fibroblasts for Western blot, we observed a faster growth of patient cells compared to healthy controls. Thus, we quantified proliferation of skin fibroblasts from families B (BIII.1 and BIII.2) and F (FII.2) versus four fibroblast cultures from passage- and age-paired controls (Fig. 4). *TRIP4*-mutant fibroblasts showed a significantly higher proliferation rate with lower mean doubling time than controls, compatible with a shorter cell cycle length (Fig. 4C). This suggested that ASC-1 might be involved in the control of cell cycle progression.

Consistently, FACS studies in non-synchronous cell cultures showed that, while most (>80%) control fibroblasts were in G0/G1 phase, there were significantly less patient cells in G0/G1 and more in S and G2 phases (Fig. 4D), indicating a significant increase of cycling cells in ASC-1 depleted cultures. Considering the cell cycle length, the G0/G1 phase was significantly shortened in patient fibroblasts compared to controls (Fig. 4E), suggesting cell cycle acceleration.

To further clarify the role of ASC-1 in myogenic cells, we used our in vitro *Trip4* knock-down (*Trip4KD*) C2C12 model, comparing cells transfected with a siRNA against *Trip4* (*siTrip4*) to those transfected with a control siRNA (Scbl) or non-transfected (NT) (Fig. 5). *siTrip4* cells showed a higher proliferation rate with a shorter doubling time compared to Scbl. Moreover, ASC-1 depleted cells were smaller. Consistently, FACS studies confirmed a decrease of cells in G0/G1 phase and a significantly reduced duration of the latter upon ASC-1 depletion. Thus, ASC-1 is involved in cell cycle regulation in both fibroblasts and myogenic cells, its depletion leading to cell cycle acceleration and reduced cell growth due to shortening of the G0/G1 phase.

### **ASC-1 depletion is associated with altered expression and phosphorylation of cell cycle exit regulators**

Cell cycle arrest is an important step in myogenic differentiation, which involves transitioning from proliferative myoblasts to post-mitotic myotubes and muscle fibers. D-type cyclins are regulators of one key G1-phase checkpoint, determining cell cycle arrest or progression into S-phase. Quantification of cyclins D1, D3 and the cell cycle exit marker p21 in frozen muscle samples from three *TRIP4*-mutant patients showed significant cyclin D1 decrease and cyclin D3 increase compared to control (Fig. 6A). p21 was significantly reduced in the two older patients. Embryonic myosin heavy chain was undetectable, suggesting that the cyclin changes in patient muscles are unlikely to be non-specifically due to muscle fiber regeneration and probably are directly associated with ASC1-related cell cycle defects in post-mitotic muscles.

Analysis of cyclins D1, D3 and p21 expression during proliferation in *Trip4KD* C2C12 myoblasts confirmed cyclin changes, showing a significant increase in cyclin D1 and p21 (Fig. 6B) without significant changes in cyclin D3 (data not shown). Increased expression of cyclin D1 and p21 in *Trip4KD* was rescued by expression of human wild-type ASC-1 (hASC-1) (Fig. 6C and data not shown), confirming that this molecular phenotype is not due to off-target effects of *Trip4* siRNA.

The Retinoblastoma Protein (pRb) interacts with cyclins and regulates both cell cycle and muscle-specific gene expression through its target E2F. Thus, abnormalities of Rb, whose activity is modulated by Cyclin/CDK-mediated phosphorylation, might be an underlying mechanism in ASC1-RM muscle phenotype. Indeed, we found an increase of the hyper-phosphorylated forms of Rb and the hyper-phosphorylated/total Rb ratio in *Trip4KD* C2C12 compared to controls (Fig. 6D). This, associated with cyclin D1 changes, could explain the rapid progression of *Trip4KD* cells from G1 to S phase and the myofibrillar abnormalities in patients' muscles, suggesting that ASC-1 is critical for controlling both cell cycle progression and myofibrillogenesis during myogenesis.

## DISCUSSION

ASC-1 related disease is emerging as a novel cause of congenital neuromuscular disorders, but its phenotypical spectrum and pathophysiology remained unclear. So far, three *TRIP4* mutations have

been described in four families with a severe neonatal phenotype (one reported as a CM, the three others as SMA)<sup>14,15</sup>. We report here five additional families with seven novel *TRIP4* mutations, expanding the phenotypical spectrum beyond lethal congenital forms to mild ambulatory adult patients.

The clinical phenotype in these families is marked by early-onset axial and proximal weakness, progressive scoliosis sometimes associated with rigid spine, dysmorphic features, cutaneous involvement and respiratory failure. No clinical, electromyographic or histological sign of motor neuron involvement was present. The severity of respiratory involvement correlated with the degree of muscle weakness, unlike in other CMs with minicores (e.g. SEPNI-Related Myopathy<sup>24,25</sup>). The skin phenotype includes skin hyperlaxity, xerosis and follicular hyperkeratosis. Remarkably, while the first patients identified never reached full ambulation, five of the novel patients are able to walk without support, being limited mainly by respiratory failure and fatigability. In the mildest case, the first referral signs were noticed in adolescence, and he remains able to climb stairs at 63 years.

Interestingly, dilated cardiomyopathy was detected in two patients in the third and fifth decades. We previously showed that *TRIP4* expression is relatively high in murine cardiac muscle<sup>14</sup>. Moreover, neonatal cardiac involvement (cardiomyopathy, atrial septal defect or patent ductus arteriosus) was reported in two SMA families with *TRIP4* mutations<sup>15</sup>. We confirm here that cardiac disease can be part of the *TRIP4*-associated phenotype, and reveal that the absence of pediatric cardiac involvement does not preclude the subsequent development of cardiomyopathy. Therefore, cardiac function should be periodically screened in all *TRIP4*-mutated patients.

Primary myocardial disease is not typical of CM, although it may appear in *TTN*-, *MYH7*- or *ACTA1*-related myopathies<sup>1</sup>. One of our patients with DCM carries a heterozygous *TTN* truncating variant (TTNtv). Heterozygous TTNtv are fairly common in the general population (up to 1%)<sup>26–28</sup> and have never been demonstrated to cause congenital skeletal muscle disease by themselves. Indeed, congenital titinopathies are autosomal recessive myopathies associated with the combination of either two truncating or one truncating and one missense *TTN* changes<sup>29–31</sup>. The TTNtv in our patient is

carried by an older sister with normal neurological and cardiological examination, and his muscle MRI is comparable to that in the other ASC1-RM patients. Thus, his skeletal muscle phenotype is most likely explained by the large homozygous *TRIP4* deletion leading to absence of ASC-1. This *TTN*tv has never been reported in DCM and does not affect the titin domains most commonly associated with cardiomyopathy<sup>28</sup>. However, a potential digenic contribution to his cardiac phenotype cannot be fully excluded at this point. In the other patient with adult-onset DCM, linkage and exomic studies excluded recessive pathogenic *TTN* changes<sup>14</sup>.

The spectrum of muscle architectural lesions in ASC1-RM is particularly large. Aside from the multi-minicores, internalized nuclei, cap lesions and mild dystrophic lesions reported<sup>14</sup>, we observed nemaline and cytoplasmic bodies in novel patients. Our findings suggest *TRIP4* as a novel culprit gene for nemaline myopathy, as well as for other forms of congenital muscle disease (including cap disease, core, centronuclear or cytoplasmic-body myopathies and congenital muscular dystrophy); therefore, we propose that it should be included in the corresponding diagnostic gene panels. Furthermore, we found in one biopsy rimmed fibers comparable to those associated with *ASCC1* mutations<sup>17</sup>. This suggests that *TRIP4* and *ASCC1* are implicated in a common pathophysiological pathway which leads to multiple forms of myofibrillar disarray, and thus to an overlap of different histopathological CM lesions.

Our phenotypical findings can be useful for differential diagnosis. The joint hyperlaxity, mild to moderate joint contractures, spinal rigidity and skin phenotype observed in some of our patients raise the question of differential diagnosis with collagen 6-related muscular dystrophies<sup>32</sup>, although *TRIP4* mutant patients had no hypertrophic scars. Moreover, minicore-like lesions may be occasionally found in patients with collagen VI-related myopathies<sup>32,33</sup>. Extraocular muscle involvement, previously unreported, may be part of the ASC1-RM spectrum but is typically absent in congenital titinopathies<sup>31</sup>. One of the patients with dilated cardiomyopathy had rigid spine and developed mild elbow contractures with age, features that overlap with Emery Dreifuss muscular dystrophy. However, the conduction defects and marked contractures typical of the latter were absent in ASC1-RM patients. In addition, muscle MRI in three ASC1-RM patients revealed a consistent pattern, with predominant

involvement of the adductor longus and posterior thigh compartment and relative preservation of the semitendinosus muscle, sometimes associated to increased subcutaneous adipose tissue<sup>14</sup>. This MRI pattern differed from the typical abnormalities associated with collagen 6 defects<sup>32,34</sup> or with other CMs with minicores such as those related to *SEPN1*<sup>35</sup>, *RYR1*<sup>36</sup> or *TTN*<sup>37</sup>, although its specificity requires confirmation by further studies.

This work significantly increases the number of known *TRIP4* mutations, confirms autosomal recessivity and defines the first genotype-phenotype correlations. The novel mutations include one large deletion and five frameshift changes predicting a reduction or absence of full-length ASC-1 protein. ASC-1 depletion was confirmed experimentally in three families, including two patients compound heterozygous for the first identified *TRIP4* missense mutation. Interestingly, ASC-1 was undetectable by Western blot both in our mildest patient and in the first severe cases reported<sup>14</sup>, suggesting other severity modulators. Additionally, the patients reported as having severe SMA<sup>15</sup> carried *TRIP4* nonsense mutations resulting in exon skipping and upregulation of a shorter isoform containing most ASC-1 functional domains. Although their muscle biopsies showed major reduction of myofiber size compatible with a primary muscle component, our findings suggest that the *TRIP4* mutations leading to ASC-1 protein depletion are associated with a primary striated muscle phenotype, while those leading to expression of a truncated protein might be associated with motoneuron disease. A better understanding of the molecular mechanisms of ASC-1 related disease should help to clarify this point.

On this note, we report a pathophysiological pathway associated with ASC-1 defects which contributes to clarify its so-far undefined role and the disease mechanism. Consistently with a muscle and skin phenotype, in the absence of ASC-1 proliferation is accelerated both in fibroblasts and myogenic cells. This increased proliferation is mainly due to a reduction of the G0/G1 phase and is associated with cell size reduction. Shortening of the G1 phase has been associated with cell size and growth reduction in mammalian cells<sup>38,39</sup> and may contribute to explain the myotube growth defect in ASC-1 depleted patient- and C2C12 cells<sup>14</sup>.

This cell cycle phenotype is associated with altered cyclin expression. In C2C12, we found that *Trip4KD* leads to an increase of cyclin D1 and p21, regulators of the G0/G1 phase, and of several downstream targets. Over-expression of D-type cyclins has been shown to shorten the G0/G1 phase<sup>40</sup>. Furthermore, the high levels of p21 and cyclin D1 in the absence of ASC-1 suggest an increased formation of the cyclin D1 and CDK4/6-complex<sup>41</sup>. This complex phosphorylates proteins such as the tumor suppressor pRb<sup>42</sup>, known to control cell cycle. Hypophosphorylated pRb inhibits E2F transcription factors required for S phase entry<sup>43</sup>. Indeed, in *Trip4KD* cells we found a consistent tendency to the reduction of the hypophosphorylated forms of pRb in favour of hyperphosphorylation, which indicates loss of pRb-mediated inhibition of the G0/G1-S transition. Interestingly, pRb activity is also necessary for late muscle development, promoting myofibrillogenesis and muscle cell growth by activating transcription of myogenic and metabolic genes<sup>44</sup>. Defects in this pathway could contribute to explain the various myofibrillar defects in patients' biopsies. Further experiments are required to corroborate pRb abnormalities and to clarify the latter point.

Cyclin D3 is a critical regulator of the proliferation/differentiation balance of myogenic progenitors in skeletal muscle<sup>45,46</sup>. Under non-pathological conditions, this protein is not expressed in adult muscle fibers, as it is more important for the establishment than the maintenance of terminal myogenic differentiation<sup>47</sup>. Cyclin D3 increase in ASC-1 depleted patients' muscles suggests a dysregulation of its expression that could be attributed to inappropriate activation by MyoD or to improper stabilization by pRb<sup>45,46</sup>. Cyclin D3 is also involved in adipogenesis through its interaction with the nuclear receptor PPAR $\gamma$ <sup>48</sup>. This could be related to the subcutaneous adiposity observed in some patients. In addition, cyclin D1 represses PPAR $\gamma$  and inhibits adipocyte differentiation<sup>49</sup>. Drastically reduced cyclin D1 in postnatal patient muscles might contribute to this adipose phenotype via PPAR $\gamma$  de-repression.

In conclusion, our work expands the clinical, histological and molecular spectrum of ASC1-RM and contributes to disentangle its pathophysiological mechanisms. We propose that *TRIP4* mutations should be considered in any patient with histopathological CM lesions and a non-contractile myopathy, even in adult ambulant patients without clear neonatal signs, particularly if the phenotype

includes respiratory insufficiency, joint hyperlaxity, skin abnormalities or cardiomyopathy. Moreover, we reveal that ASC-1 plays a key role not only in late stages of myogenic differentiation and myotube growth<sup>14</sup> but also as a novel cell-cycle regulator in several cell types, controlling cell proliferation via regulation of key cell-cycle proteins. This work confirms transcriptional co-regulation defects as an emerging mechanism in inherited neuromuscular disease. Based on the identification of common histopathological lesions in *TRIP4*- and *ASCC1*-mutant patients, we propose the term ‘ASC1-related myopathies’ to include pathologies associated with both genes and with potential defects of any other protein of the ASC-1 complex, whose relevance in muscle and/or motoneuron pathophysiology is likely to increase in the future.

For Peer Review

## ACKNOWLEDGMENTS

The authors wish to thank the patients and their families for their cooperation. We also want to thank Dr Miguel Iniesto (Université Paris Sud) for assistance in statistical analysis. We acknowledge the ImagoSeine core facility of the Institut Jacques Monod, member of the France BioImaging (ANR-10-INSB-04) and the support of La ligue contre le Cancer (R03/75-79). Microscopy analyses were performed on the 'Plateau imagerie' facility of the Functional and Adaptive Biology Unit (BFA), Université de Paris/CNRS, Sorbonne Paris Cité, France. We thank MYOBANK-AFM (Institut de Myologie, BB-0033-00012) and the Banque de Cellules et d'ADN (Genethon, Evry, France) for the disposal of biological samples and their contribution to human cell cultures, respectively.

This work was funded by the Association Française contre les Myopathies (AFM, Grants #20923 and #21267), the Institut National de la Santé et la Recherche Médicale (Inserm), the Centre National de la Recherche Scientifique (CNRS) and the Université de Paris, France. R.N.V.Q. is the recipient of a research grant from the Alfonso Martín Escudero Foundation (Beca de investigación en universidades o centros en el extranjero, Convocatoria 2017). M.O. is supported by the "Instituto de Salud Carlos III" through the project PI14/00738 (co-funded by European Regional Development Fund ERDF, a way to build Europe). WES and analysis of Family C were supported by National Institutes of Health (USA) grants UM1 HG008900 and R01 HD075802 and MDA602235 from the Muscular Dystrophy Association (USA). Sanger confirmation for family C was performed by the Molecular Genetics Core of the Boston Children's Hospital IDDRC funded by National Institutes of Health grant U54 HD090255.

## AUTHOR CONTRIBUTIONS

AF, IDG and RNVQ conceived and designed this study. Acquisition and analysis of data were performed by RNVQ, FC, RJM, CAG, TG, AK, AY, SC, EPH, JR, NBR, AHB, LS, MC, MO, XL, JD, JB, IDG and AF. ND and JL contributed to discussions. RNVQ, IDG, AF were responsible for drafting the manuscript and figure preparation. All authors read and approved the final manuscript.

## POTENTIAL CONFLICTS OF INTEREST

The authors declare that they have no conflict of interest.

## REFERENCES

1. North KN, Wang CH, Clarke N, et al. Approach to the diagnosis of congenital myopathies. *2017;24(2):97–116.*
2. Schorling D, Kirschner J, Bönnemann C. Congenital Muscular Dystrophies and Myopathies: An Overview and Update [Internet]. *Neuropediatrics 2017;48(4):247–261.*
3. Wang CH, Quijano-roy S, Deconinck N, et al. Diagnostic approach to the congenital muscular dystrophies. *HHS Public Access ,Neuromuscul Disord 2017;24(4):289–311.*
4. Jungbluth H, Ochala J, Treves S, Gautel M. Current and future therapeutic approaches to the congenital myopathies. *Semin. Cell Dev. Biol. 2017;64:191–200.*
5. Kaplan J-C, Hamroun D. The 2016 version of the gene table of monogenic neuromuscular disorders (nuclear genome). *Neuromuscul. Disord. 2015;25(12):991–1020.*[
6. Ravenscroft G, Laing NG, Bönnemann CG. Pathophysiological concepts in the congenital myopathies: blurring the boundaries, sharpening the focus. *Brain 2015;138(Pt 2):246–68.*
7. Treves S, Jungbluth H, Voermans N, et al. Ca<sup>2+</sup> handling abnormalities in early-onset muscle diseases: Novel concepts and perspectives. *Semin. Cell Dev. Biol. 2017;64:201–212.*
8. Horstick EJ, Linsley JW, Dowling JJ, et al. *Stac3* is a component of the excitation–contraction coupling machinery and mutated in Native American myopathy. *Nat. Commun. 2013;4(1):1952.*
9. Dowling JJ, Lawlor MW, Dirksen RT. Triadopathies: an emerging class of skeletal muscle diseases. *Neurotherapeutics 2014;11(4):773–85.*
10. Jungbluth H, Gautel M. Pathogenic Mechanisms in Centronuclear Myopathies. *Front. Aging Neurosci. 2014;6:339.*
11. Wallgren-Pettersson C, Sewry CA, Nowak KJ, Laing NG. Nemaline Myopathies. *Semin. Pediatr. Neurol. 2011;18(4):230–238.*
12. Tajsharghi H, Oldfors A. Myosinopathies: pathology and mechanisms. *Acta Neuropathol. 2013;125(1):3–18.*
13. Jungbluth H, Treves S, Zorzato F, et al. Congenital myopathies: disorders of excitation–contraction coupling and muscle contraction. *Nat. Rev. Neurol. 2018; 14(3), 151.*
14. Davignon L, Chauveau C, Julien C, et al. The transcription coactivator ASC-1 is a regulator of skeletal myogenesis, and its deficiency causes a novel form of congenital muscle disease. *Hum. Mol. Genet. 2016;25(8):1559–1573.*
15. Knierim E, Hirata H, Wolf NI, et al. Mutations in Subunits of the Activating Signal Cointegrator 1 Complex Are Associated with Prenatal Spinal Muscular Atrophy and Congenital Bone Fractures. *Am. J. Hum. Genet. 2016;98(3):473–489.*

16. Oliveira J, Martins M, Pinto Leite R, et al. The new neuromuscular disease related with defects in the ASC-1 complex: report of a second case confirms *ASCC1* involvement. *Clin. Genet.* 2017;92(4):434–439.
17. Böhm J, Malfatti E, Oates E, et al. Novel *ASCC1* mutations causing prenatal-onset muscle weakness with arthrogryposis and congenital bone fractures. *J. Med. Genet.* 2018;jmedgenet-2018-105390.
18. Dasgupta S, Lonard DM, O'Malley BW. Nuclear receptor coactivators: master regulators of human health and disease. [Internet]. *Annu. Rev. Med.* 2014;65(1):279–92.[cited 2018 Jun 26 ] Available from: <http://www.annualreviews.org/doi/10.1146/annurev-med-051812-145316>
19. Jung D-J, Sung H-S, Goo Y-W, et al. Novel Transcription Coactivator Complex Containing Activating Signal Cointegrator 1. *Mol. Cell. Biol.* 2002;22(14):5203–5211.
20. Kim HJ, Yi JY, Sung HS, et al. Activating signal cointegrator 1, a novel transcription coactivator of nuclear receptors, and its cytosolic localization under conditions of serum deprivation. *Mol. Cell. Biol.* 1999;19(9):6323–32.
21. Auboeuf D, Hönig A, Berget SM, O'Malley BW. Coordinate regulation of transcription and splicing by steroid receptor coregulators. *Science* 2002;298(5592):416–9.
22. Iyer LM, Burroughs AM, Aravind L. The ASCH superfamily: novel domains with a fold related to the PUA domain and a potential role in RNA metabolism. *Bioinformatics* 2006;22(3):257–63.
23. Chi B, O'Connell JD, Iocolano AD, et al. The neurodegenerative diseases ALS and SMA are linked at the molecular level via the ASC-1 complex. *Nucleic Acids Res.* 2018;46(22):11939–11951.
24. Ferreira A, Quijano-Roy S, Pichereau C, et al. Mutations of the selenoprotein N gene, which is implicated in rigid spine muscular dystrophy, cause the classical phenotype of multiminicore disease: reassessing the nosology of early-onset myopathies. *Am. J. Hum. Genet.* 2002;71(4):739–49.
25. Scoto M, Cirak S, Mein R, et al. *SEPN1*-related myopathies: Clinical course in a large cohort of patients. *Neurology* 2011;76(24):2073–2078.
26. Ware JS, Cook SA. Role of titin in cardiomyopathy: from DNA variants to patient stratification. *Nat. Rev. Cardiol.* 2017;15(4):241–252.
27. Franaszczyk M, Chmielewski P, Truszkowska G, et al. Titin Truncating Variants in Dilated Cardiomyopathy – Prevalence and Genotype-Phenotype Correlations. *PLoS One* 2017;12(1):e0169007.
28. Schafer S, de Marvao A, Adami E, et al. Titin-truncating variants affect heart function in disease cohorts and the general population. *Nat. Genet.* 2017;49(1):46–53.
29. Savarese M, Maggi L, Vihola A, et al. Interpreting Genetic Variants in Titin in Patients With Muscle Disorders. *JAMA Neurol.* 2018;75(5):557.
30. Chauveau C, Rowell J, Ferreira A. A rising titan: TTN review and mutation update. *Hum. Mutat.* 2014;35(9):1046–59.
31. Oates EC, Jones KJ, Donkervoort S, et al. Congenital Titinopathy: Comprehensive characterization and pathogenic insights. *Ann. Neurol.* 2018;83(6):1105–1124.
32. Bönnemann CG. The collagen VI-related myopathies: muscle meets its matrix. *Nat. Rev.*

- Neurol. 2011;7(7):379–390.
33. Bönnemann CG. The collagen VI-related myopathies [Internet]. In: Handbook of clinical neurology. 2011 p. 81–96.
  34. Mercuri E, Lampe A, Allsop J, et al. Muscle MRI in Ullrich congenital muscular dystrophy and Bethlem myopathy. *Neuromuscul. Disord.* 2005;15(4):303–310.
  35. Hankiewicz K, Carlier RY, Lazaro L, et al. Whole-body muscle magnetic resonance imaging in SEPN1-related myopathy shows a homogeneous and recognizable pattern. *Muscle Nerve* 2015;52(5):728–35.
  36. Jungbluth H, Davis MR, Müller C, et al. Magnetic resonance imaging of muscle in congenital myopathies associated with RYR1 mutations. *Neuromuscul. Disord.* 2004;14(12):785–790.
  37. Carlier R-Y, Quijano-Roy S. Myoimaging in Congenital Myopathies. *Semin. Pediatr. Neurol.* 2019;29:30–43.
  38. Jiang W, Kahn SM, Zhou P, et al. Overexpression of cyclin D1 in rat fibroblasts causes abnormalities in growth control, cell cycle progression and gene expression. *Oncogene* 1993;8(12):3447–57.
  39. Cadart C, Monnier S, Grilli J, et al. Size control in mammalian cells involves modulation of both growth rate and cell cycle duration. *Nat. Commun.* 2018;9(1):3275.
  40. Buttitta LA, Edgar BA. Mechanisms controlling cell cycle exit upon terminal differentiation. *Curr. Opin. Cell Biol.* 2007;19(6):697–704.
  41. LaBaer J, Garrett MD, Stevenson LF, et al. New functional activities for the p21 family of CDK inhibitors. *Genes Dev.* 1997;11(7):847–862.
  42. Ezhevsky SA, Ho A, Becker-Hapak M, et al. Differential regulation of retinoblastoma tumor suppressor protein by G(1) cyclin-dependent kinase complexes in vivo. *Mol. Cell. Biol.* 2001;21(14):4773–84.
  43. Leshem Y, Halevy O. Phosphorylation of pRb is required for HGF-induced muscle cell proliferation and is p27kip1-dependent. *J. Cell. Physiol.* 2002;191(2):173–182.
  44. Zappia MP, Rogers A, Islam ABMMK, Frolov M V. Rbf Activates the Myogenic Transcriptional Program to Promote Skeletal Muscle Differentiation. *Cell Rep.* 2019;26(3):702–719.e6.
  45. Cenciarelli C, De Santa F, Puri PL, et al. Critical Role Played by Cyclin D3 in the MyoD-Mediated Arrest of Cell Cycle during Myoblast Differentiation. *Mol. Cell. Biol.* 1999;19(7):5203–5217.
  46. De Santa F, Albini S, Mezzaroma E, et al. pRb-dependent cyclin D3 protein stabilization is required for myogenic differentiation. *Mol. Cell. Biol.* 2007;27(20):7248–65.
  47. Bartkova J, Lukas J, Strauss M, Bartek J. Cyclin D3: requirement for G1/S transition and high abundance in quiescent tissues suggest a dual role in proliferation and differentiation. *Oncogene* 1998;17(8):1027–1037.
  48. Sarruf DA, Iankova I, Abella A, et al. Cyclin D3 promotes adipogenesis through activation of peroxisome proliferator-activated receptor gamma. *Mol. Cell. Biol.* 2005;25(22):9985–95.
  49. Fu M, Rao M, Bouras T, et al. Cyclin D1 Inhibits Peroxisome Proliferator-activated Receptor  $\gamma$ -mediated Adipogenesis through Histone Deacetylase Recruitment. *J. Biol. Chem.*

2005;280(17):16934–16941.

For Peer Review

## FIGURE LEGENDS

**Fig. 1: ASC-1 Related Myopathy phenotypical spectrum.** (A) Clinical findings in patients CIII.7 (a), DII.2 (b-f) and EII.4 (g,h). (a) Congenital presentation with neonatal hypotonia (frog position), poor limb movements and respiratory distress requiring tracheostomy and assisted ventilation. He had skin lesions, dysmorphic facial features (i.e flat face; not shown) and tapering fingers. (b-f) Patient DII.2, still ambulant at age 35 years: note severe scoliosis with dorsal lordosis and unbalanced hips (b,d), thoracic deformities (pectus excavatum) and elbow contractures (b) contrasting with prominent joint hyperlaxity (f). Dysmorphic features included large, thick neck and retrognathism and low-set ears (not shown). The skin phenotype was marked by follicular hyperkeratosis, xerosis with scratch lesions, prominent scars (but not keloid) and skin hyperelasticity (c,e). (g,h): The mildest patient (EII.4), still ambulant at 63 years, has proximal amyotrophy, pectus excavatum and dysmorphic facial features (flat face, thick neck, retrognathia). (B) Muscle imaging in two patients revealed predominant involvement of posterior thigh compartment with relative preservation of the semitendinosus muscle. (a-c): Lower limb MRI from a mild patient (BIII.1), still ambulant at age 19 years. Axial T1-weighted images showed mild muscle atrophy and fatty infiltration of glutei, iliopsoas and posterior thigh muscles with major involvement of adductor longus and relative preservation of gracillis, sartorius and semitendinosus muscles (arrows). Note marked increase in subcutaneous adipose tissue. (d-g): Muscle MRI from patient EII.4 (aged 56 years), showed the same pattern, including fatty infiltration of paravertebral muscles (d) and the posterior thigh compartment, notably gluteus maximus, adductor longus and semimembranosus (e,f). Note relative preservation of semitendinosus. Leg muscles showed diffuse involvement (g).

**Fig. 2: Spectrum of histopathological lesions.** Skeletal muscle biopsies from patients CIII.7 (a), AIII.2 (b-d, g), EII.4 (f, h-j) and DII.2 (e, k). Muscle biopsy from the most severe patient (a) showed mildly increased endomysial connective tissue, a subpopulation of very small fibers and abundant fibers with apparently normal diameter and centrally located nuclei (arrowheads). In milder patients, dystrophic features were absent and the pattern was more typical of a congenital myopathy, including

FSV (b,c), internalized nuclei, often central, (c, black arrowheads), whorled fibers (c, white arrowheads) and type 1 fiber predominance (b). Intense oxidative rims beneath the sarcolemma, compatible with mitochondrial proliferation or mislocalization, were found in one patient in NADH-TR (e) and also in SDH and COX stains (not shown). There were multiple areas lacking oxidative activity (pink arrows in d) and showing mitochondrial depletion and sarcomere disorganization on EM (minicores) (g, k). Modified Gomori trichrome revealed purple stained lesions (f) which corresponded to electron-dense nemaline rods (h, j) on EM. Subsarcolemmal myofibrillar disorganization along with cytoplasmic bodies and/or subsarcolemmal rods were also observed (i). Transversal frozen sections, HE (a,c), ATPase pH 9.4 (b), NADH-TR (d,e), modified Gomori trichrome (f); electron microscopy (EM) (g-k). Scale bars= 25  $\mu\text{m}$  (a,b), 50  $\mu\text{m}$  (c,d), 25  $\mu\text{m}$  (e,f), 10  $\mu\text{m}$  (g), 1  $\mu\text{m}$  (h), 2  $\mu\text{m}$  (i,k), 500 nm (j).

**Fig. 3: *TRIP4* mutations in the novel families.** (A) Pedigree of novel families. (B) Summary of the mutations identified. dbSNP: Single Nucleotide Polymorphism Database. ExAC: Exome Aggregation Consortium. (C) Schematic representation of the ASC-1 protein and localization of the patients' mutations. (D-E) ASC-1 expression in patient samples. (D) Low expression of full-length ASC-1 (arrow) in fibroblasts from patients BIII.1 and BIII.2. (E) Full-length ASC-1 (arrows) was undetectable in muscle biopsies from patient DII.2 and EII.4. ctl: control fibroblasts (D), skeletal muscle control (E).

**Fig. 4: Accelerated proliferation and reduced G0/G1 phase of the cell cycle in patient fibroblasts.** (A) Bright-field pictures of control (Ctl1) and patient (BIII.2) fibroblasts cultures from 24 to 96 hours after seeding (B) proliferation curves from four control (blue) and three patient fibroblasts cultures (red). (C) Differences between the proliferation curves from control and patient cells were significant (ANOVA 3DF, \*p-value<0.001). Mean population doubling time of control and patient cells was calculated for cells in exponential proliferation between 48 and 72h. (D) FACS analysis of cell cycle progression in non-synchronous proliferative control (Ctl1) or patient (BIII.1; FII.2) fibroblasts. Histogram showing the mean percentage of cells per phase in the four controls and three patients

fibroblast samples (ANOVA 2DF,  $p$ -value  $<0.001$ ; Tukey HSD \* $p$ -value 0.01 \*\* $p$ -value 0.002). (E) The duration of cell cycle phases G0/G1 (blue), S (yellow) and G2M (green) for each sample was determined as the percentage of cells in each phase multiplied by the doubling time corresponding to each sample.

**Fig. 5: Accelerated proliferation and G0/G1 phase reduction and reduced growth in *Trip4*KD myogenic cells.** (A) Bright-field pictures of *Trip4*KD C2C12 (*siTrip4*) compared to not treated (NT) or scramble (Scbl) transfected controls from 24 to 72 hours post siRNA transfection. (B) Proliferation curves of *siTrip4*, Scbl and NT cells. Overall, the proliferation curve of *siTrip4* cells was higher than that from Scbl-transfected controls (ANOVA, \*\* $p$ -value  $<0.001$ ), maintaining values comparable to non-transfected cells. Values are the mean of four independent measurements for each time per condition. Mean population doubling time (hours) was calculated for cells in exponential proliferation between 24 and 48h after transfection: NT  $16.6 \pm 1$ , Scbl  $20.1 \pm 4.4$ , *siTrip4*  $15.1 \pm 1.5$ . (C) *SiTrip4* cells exhibited a smaller cell surface ( $\mu\text{m}^2$ ) compared to NT or Scbl cells after 24, 48 or 72h of culture (Kruskal-Wallis, \* $p$ -value  $< 0.05$ ). A strong ASC-1 reduction ( $>80\%$ ) of ASC-1 in *Trip4*KD cells was observed 48h after transfection. This was also observed within 48 hours with three independent siRNAs against *Trip4* (data not shown). (D) FACS analysis of cell cycle in non-synchronous NT, Scbl and *siTrip4* cells. Mean cell cycle distributions measured in three experiments showed a decrease in the percentage of cells in G0/G1 phase in *siTrip4* condition compared to Scbl and NT (respectively  $51 \pm 3.3$ ;  $54.3 \pm 6.1$ ;  $60.1 \pm 4.7$ ), an increase in S phase (respectively  $36.4 \pm 2.3$ ;  $35.6 \pm 3.9$ ;  $29.1 \pm 3.7$ ) and in G2M (respectively  $10.8 \pm 1.3$ ;  $9.64 \pm 1.1$ ;  $9.74 \pm 2.3$ ). The duration of the cell cycle phases ( $\pm$ SEM), G0/G1 (blue), S (yellow) and G2M (green), was determined as mentioned in Fig. 4 (ANOVA \* $p$ -value  $<0.05$ ). A parallel increase in the number of cells in S phase in both Scbl and *siTrip4* samples could be explained by the stress induced by transfection.

**Fig. 6: Altered expression of cell cycle proteins in patient muscles and in *Trip4*KD myogenic cells.** (A) Western blot of lysates from control (ctl) and three patient frozen muscles revealed altered expression of cyclins D1 and D3 as well as p21 in patients DII.2 (left panel), EII.4 and FIII.1 (right panel, control expression normalized to 1, dashed line). Absence of embryonic myosin (MHCE) in

both patient DII.2 and control muscle samples excluded that this might be due to active muscle regeneration (including the presence of immature myofibers) in patients (lower panel, C2C12 used as a positive control). (B) Increased cyclin D1 and p21 expression in *Trip4*KD C2C12 with <20% ASC-1 residual expression (data not shown) compared to non-transfected cells (NT) or cells transfected with siRNA control (Scbl) (left and right panel, normalized to Scbl transfected cells; Mann–Whitney U, \*p-value <0.05). (C) Rescue of the altered levels of cyclin D1 in *Trip4*KD C2C12 by wild-type human ASC-1. Western blot of protein extracts from Scbl (lanes 1 and 4), *siTrip4* (lanes 2 and 5) or ctl C2C12 (lane 3) double-transfected with hASC-1 (lanes 3-5) 24h after endogenous ASC-1 silencing (upper panel). Quantification of the relative expression of cyclin D1 over tubulin (normalized for Scbl) in ctl, Scbl and *siTrip4* cells in the presence or absence of hASC-1. A vector expressing hCelf1 was used as a non-specific control (lower panel). mASC-1= murine endogenous ASC-1; hASC-1 = human ectopic ASC-1; hCelf1 = human ectopic Celf1. (D) Western blot analysis of pRb phosphorylation state in NT, Scbl and *siTrip4* cells revealed a fast migrating band corresponding to the hypo-phosphorylated form of Rb (pRb, 110 kDa) and slower migrating bands corresponding to hyper-phosphorylated forms of Rb (ppRb, 116kDa) (left panel). Red ponceau (redP) staining of the membrane showed similar loading in each condition. In all conditions, the hyper-phosphorylated forms of Rb were predominant compared to the hypo-phosphorylated form as expected for cycling cells. Although variability precluded reaching statistical significance, quantification of the ratio ppRb/total pRb for each condition (N=4) showed an increase by nearly 50% of hyper-phosphorylated forms in *siTrip4* cells (right panel).



Figure 1. ASC-1 Related Myopathy phenotypical spectrum. (A) Clinical findings in patients CIII.7 (a), DII.2 (b-f) and EII.4 (g,h). (a) Congenital presentation with neonatal hypotonia (frog position), poor limb movements and respiratory distress requiring tracheostomy and assisted ventilation. He had skin lesions, dysmorphic facial features (i.e flat face; not shown) and tapering fingers. (b-f) Patient DII.2, still ambulant at age 35 years: note severe scoliosis with dorsal lordosis and unbalanced hips (b,d), thoracic deformities (pectus excavatum) and elbow contractures (b) contrasting with prominent joint hyperlaxity (f). Dysmorphic features included large, thick neck and retrognathism and low-set ears (not shown). The skin phenotype was marked by follicular hyperkeratosis, xerosis with scratch lesions, prominent scars (but not keloid) and skin hyperelasticity (c,e). (g,h): The mildest patient (EII.4), still ambulant at 63 years, has proximal amyotrophy, pectus excavatum and dysmorphic facial features (flat face, thick neck, retrognathia). (B) Muscle imaging in two patients revealed predominant involvement of posterior thigh compartment with relative preservation of the semitendinosus muscle. (a-c): Lower limb MRI from a mild patient (BIII.1), still ambulant at age 19 years. Axial T1-weighted images showed mild muscle atrophy and fatty infiltration of glutei, iliopsoas and posterior thigh muscles with major involvement of adductor longus and relative

preservation of gracilis, sartorius and semitendinosus muscles (arrows). Note marked increase in subcutaneous adipose tissue. (d-g): Muscle MRI from patient EII.4 (aged 56 years), showed the same pattern, including fatty infiltration of paravertebral muscles (d) and the posterior thigh compartment, notably gluteus maximus, adductor longus and semimembranosus (e,f). Note relative preservation of semitendinosus. Leg muscles showed diffuse involvement (g).

167x197mm (300 x 300 DPI)

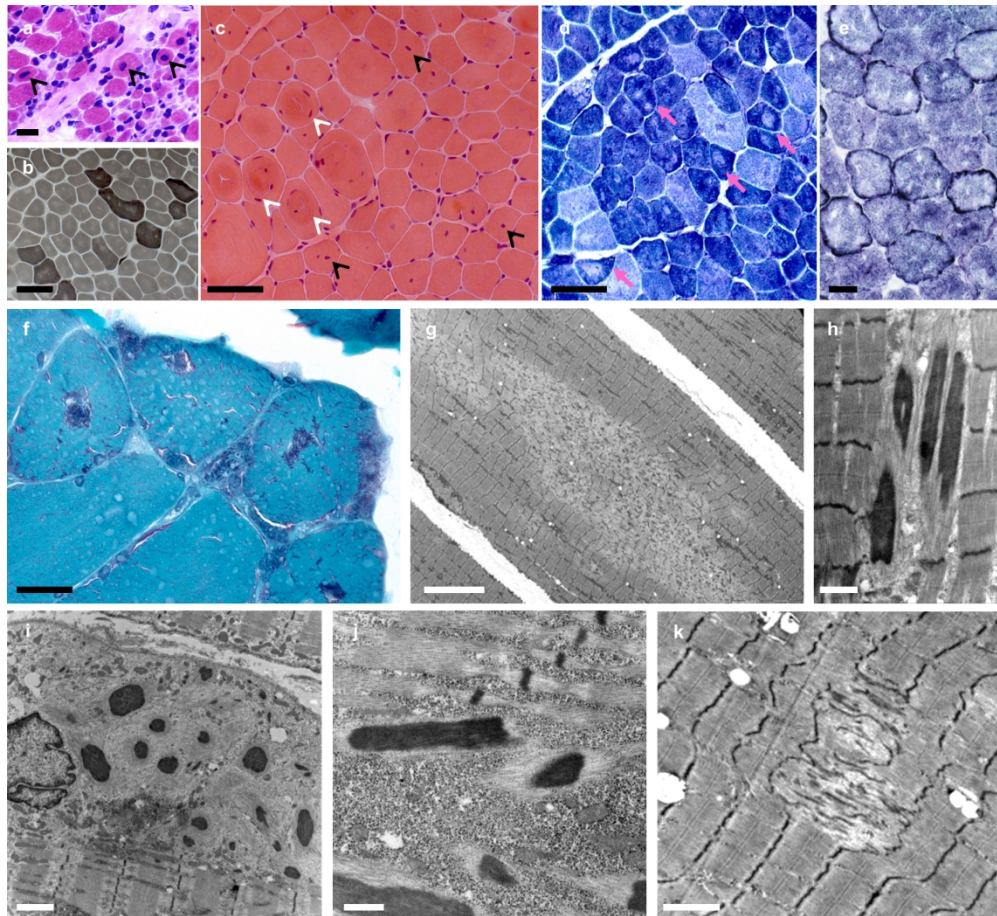


Figure 2. Spectrum of histopathological lesions. Skeletal muscle biopsies from patients CIII.7 (a), AIII.2 (b-d, g), EII.4 (f, h-j) and DII.2 (e, k). Muscle biopsy from the most severe patient (a) showed mildly increased endomysial connective tissue, a subpopulation of very small fibers and abundant fibers with apparently normal diameter and centrally located nuclei (arrowheads). In milder patients, dystrophic features were absent and the pattern was more typical of a congenital myopathy, including FSV (b,c), internalized nuclei, often central, (c, black arrowheads), whorled fibers (c, white arrowheads) and type 1 fiber predominance (b). Intense oxidative rims beneath the sarcolemma, compatible with mitochondrial proliferation or mislocalization, were found in one patient in NADH-TR (e) and also in SDH and COX stains (not shown). There were multiple areas lacking oxidative activity (pink arrows in d) and showing mitochondrial depletion and sarcomere disorganization on EM (minicores) (g, k). Modified Gomori trichrome revealed purple stained lesions (f) which corresponded to electron-dense nemaline rods (h, j) on EM. Subsarcolemmal myofibrillar disorganization along with cytoplasmic bodies and/or subsarcolemmal rods were also observed (i). Transversal frozen sections, HE (a,c), ATPase pH 9.4 (b), NADH-TR (d,e), modified Gomori trichrome (f); electron microscopy (EM) (g-k). Scale bars= 25  $\mu$ m (a,b), 50  $\mu$ m (c,d), 25  $\mu$ m (e,f), 10  $\mu$ m (g), 1  $\mu$ m (h), 2  $\mu$ m (i,k), 500 nm (j).

170x155mm (300 x 300 DPI)

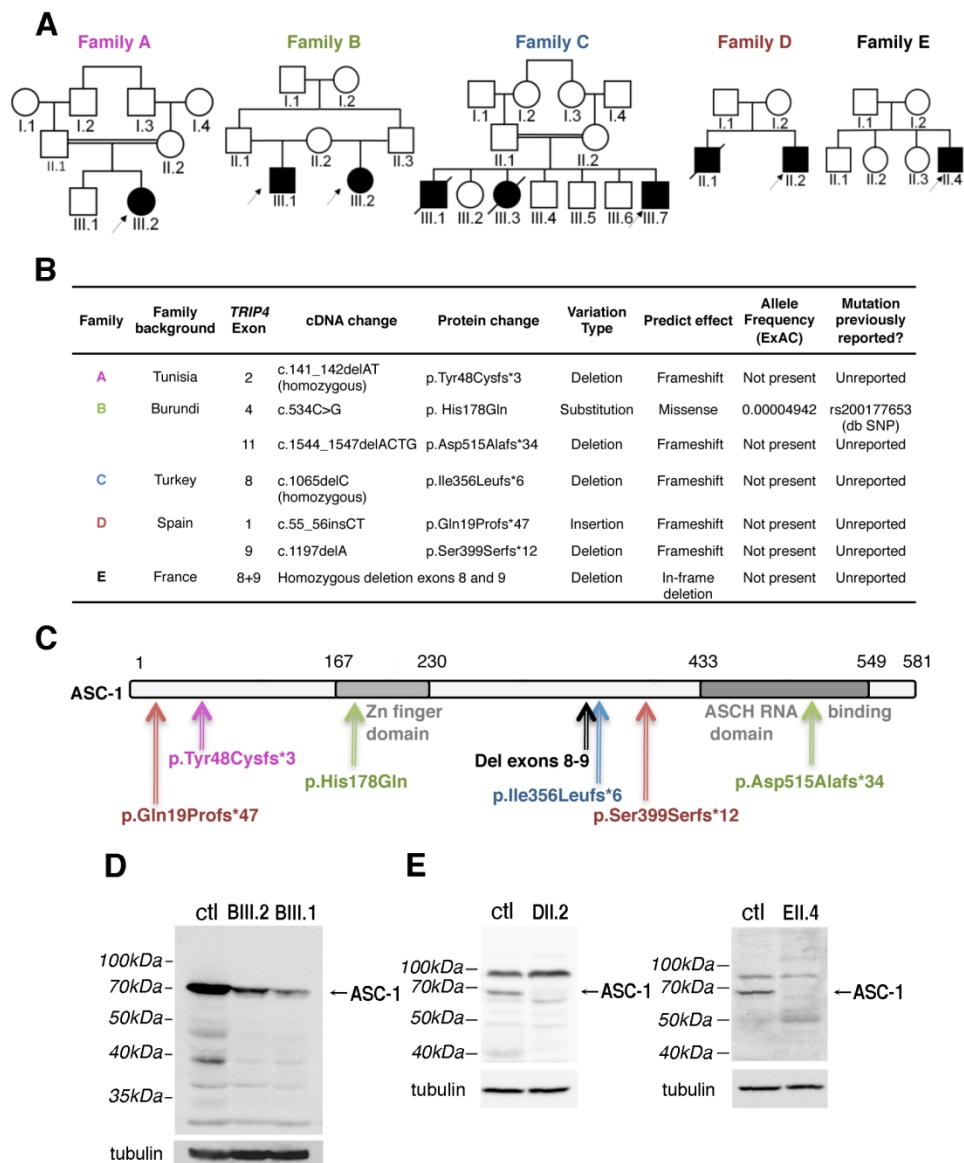


Figure 3. TRIP4 mutations in the novel families. (A) Pedigree of novel families. (B) Summary of the mutations identified. dbSNP: Single Nucleotide Polymorphism Database. ExAC: Exome Aggregation Consortium. (C) Schematic representation of the ASC-1 protein and localization of the patients' mutations. (D-E) ASC-1 expression in patient samples. (D) Low expression of full-length ASC-1 (arrow) in fibroblasts from patients BIII.1 and BIII.2. (E) Full-length ASC-1 (arrows) was undetectable in muscle biopsies from patient DII.2 and EII.4. ctl: control fibroblasts (D), skeletal muscle control (E).

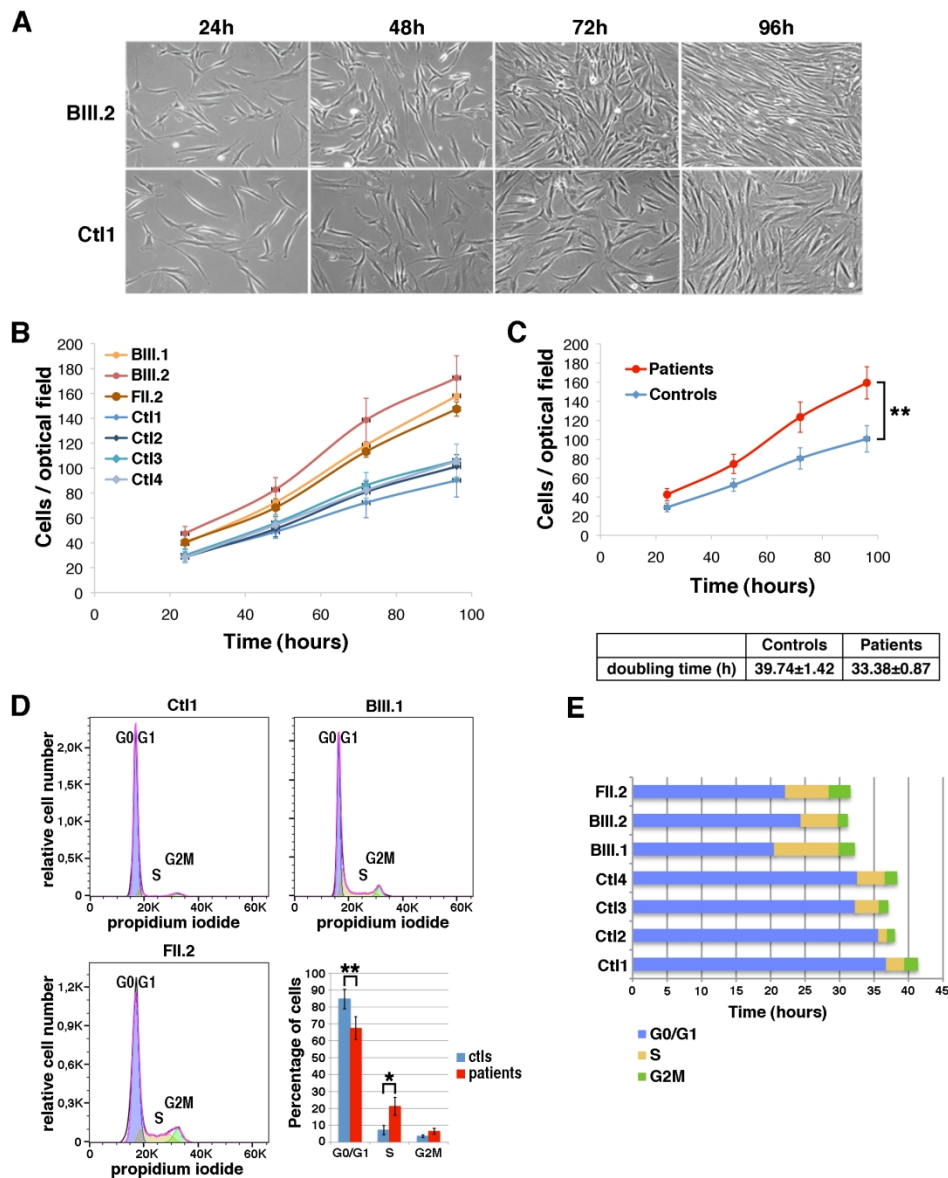


Figure 4. Accelerated proliferation and reduced G0/G1 phase of the cell cycle in patient fibroblasts. (A) Bright-field pictures of control (Ctl1) and patient (BIII.2) fibroblasts cultures from 24 to 96 hours after seeding (B) proliferation curves from four control (blue) and three patient fibroblasts cultures (red). (C) Differences between the proliferation curves from control and patient cells were significant (ANOVA 3DF, \*p-value<0.001). Mean population doubling time of control and patient cells was calculated for cells in exponential proliferation between 48 and 72h. (D) FACS analysis of cell cycle progression in non-synchronous proliferative control (Ctl1) or patient (BIII.1; FII.2) fibroblasts. Histogram showing the mean percentage of cells per phase in the four controls and three patients fibroblast samples (ANOVA 2DF, p-value<0.001; Tukey HSD \*p-value 0.01 \*\*p-value 0.002). (E) The duration of cell cycle phases G0/G1 (blue), S (yellow) and G2M (green) for each sample was determined as the percentage of cells in each phase multiplied by the doubling time corresponding to each sample.

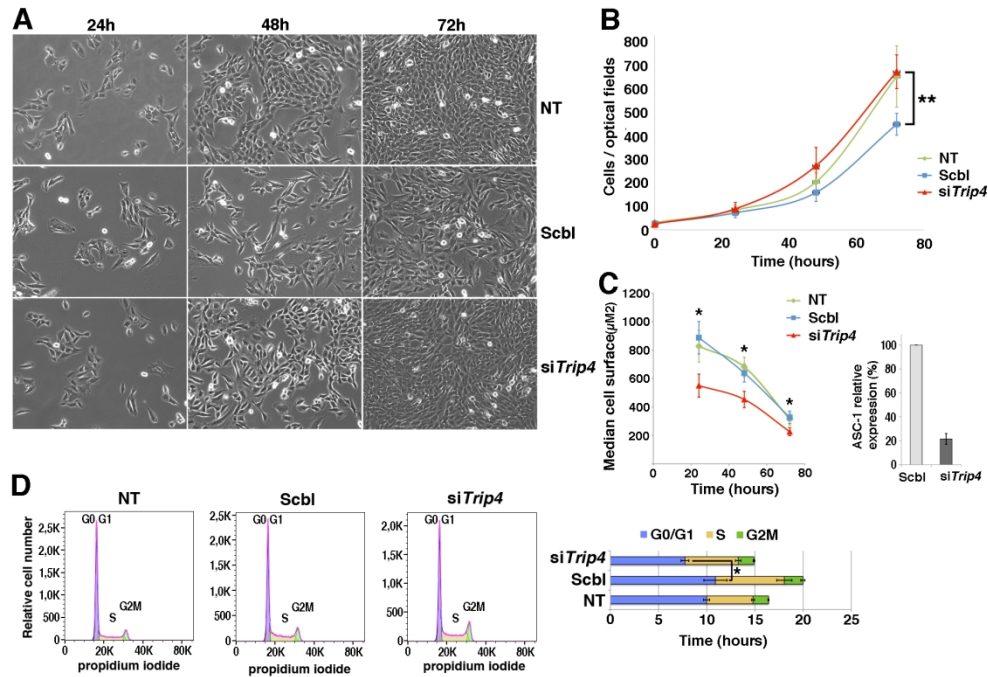


Figure 5. Accelerated proliferation and G0/G1 phase reduction and reduced growth in Trip4KD myogenic cells. (A) Bright-field pictures of Trip4KD C2C12 (siTrip4) compared to not treated (NT) or scramble (Scbl) transfected controls from 24 to 72 hours post siRNA transfection. (B) Proliferation curves of siTrip4, Scbl and NT cells. Overall, the proliferation curve of siTrip4 cells was higher than that from Scbl-transfected controls (ANOVA, \*\*p-value <0.001), maintaining values comparable to non-transfected cells. Values are the mean of four independent measurements for each time per condition. Mean population doubling time (hours) was calculated for cells in exponential proliferation between 24 and 48h after transfection: NT  $16.6 \pm 1$ , Scbl  $20.1 \pm 4.4$ , siTrip4  $15.1 \pm 1.5$ . (C) SiTrip4 cells exhibited a smaller cell surface ( $\mu\text{m}^2$ ) compared to NT or Scbl cells after 24, 48 or 72h of culture (Kruskal-Wallis, \*p-value < 0.05). A strong ASC-1 reduction (>80%) of ASC-1 in Trip4KD cells was observed 48h after transfection. This was also observed within 48 hours with three independent siRNAs against Trip4 (data not shown). (D) FACS analysis of cell cycle in non-synchronous NT, Scbl and siTrip4 cells. Mean cell cycle distributions measured in three experiments showed a decrease in the percentage of cells in G0/G1 phase in siTrip4 condition compared to Scbl and NT (respectively  $51 \pm 3.3$ ;  $54.3 \pm 6.1$ ;  $60.1 \pm 4.7$ ), an increase in S phase (respectively  $36.4 \pm 2.3$ ;  $35.6 \pm 3.9$ ;  $29.1 \pm 3.7$ ) and in G2M (respectively  $10.8 \pm 1.3$ ;  $9.64 \pm 1.1$ ;  $9.74 \pm 2.3$ ). The duration of the cell cycle phases ( $\pm$ SEM), G0/G1 (blue), S (yellow) and G2M (green), was determined as mentioned in Fig. 4 (ANOVA \*p-value <0.05). A parallel increase in the number of cells in S phase in both Scbl and siTrip4 samples could be explained by the stress induced by transfection.

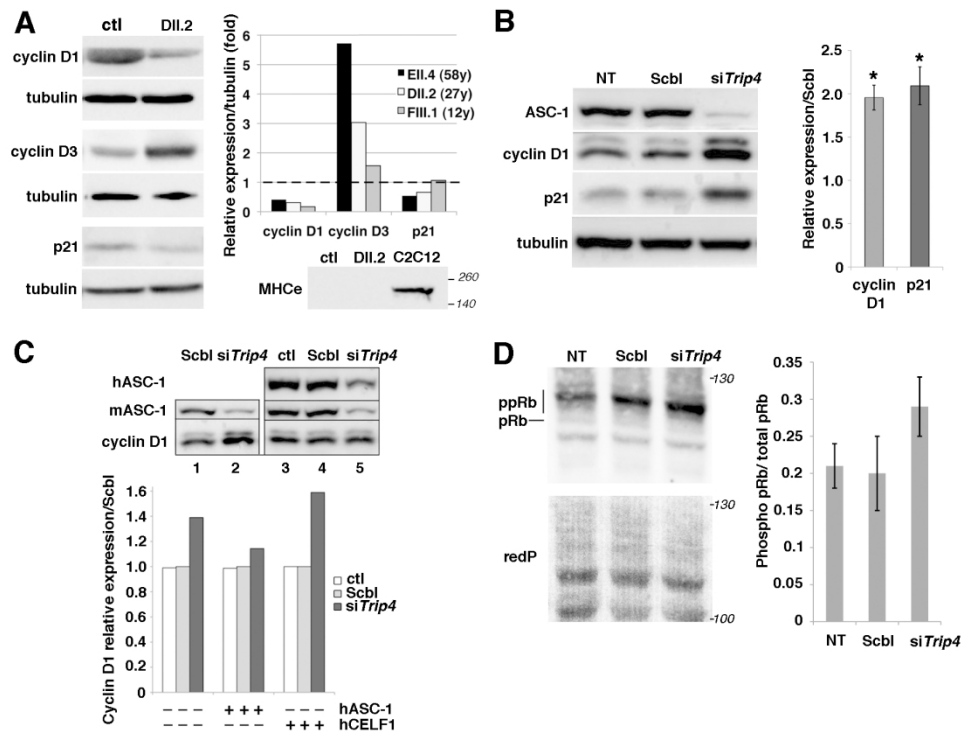


Figure 6. Altered expression of cell cycle proteins in patient muscles and in Trip4KD myogenic cells. (A) Western blot of lysates from control (ctl) and three patient frozen muscles revealed altered expression of cyclins D1 and D3 as well as p21 in patients DII.2 (left panel), EII.4 and FIII.1 (right panel, control expression normalized to 1, dashed line). Absence of embryonic myosin (MHCE) in both patient DII.2 and control muscle samples excluded that this might be due to active muscle regeneration (including the presence of immature myofibers) in patients (lower panel, C2C12 used as a positive control). (B) Increased cyclin D1 and p21 expression in Trip4KD C2C12 with <20% ASC-1 residual expression (data not shown) compared to non-transfected cells (NT) or cells transfected with siRNA control (Scbl) (left and right panel, normalized to Scbl transfected cells; Mann-Whitney U, \*p-value <0.05). (C) Rescue of the altered levels of cyclin D1 in Trip4KD C2C12 by wild-type human ASC-1. Western blot of protein extracts from Scbl (lanes 1 and 4), siTrip4 (lanes 2 and 5) or ctl C2C12 (lane 3) double-transfected with hASC-1 (lanes 3-5) 24h after endogenous ASC-1 silencing (upper panel). Quantification of the relative expression of cyclin D1 over tubulin (normalized for Scbl) in ctl, Scbl and siTrip4 cells in the presence or absence of hASC-1. A vector expressing hCelf1 was used as a non-specific control (lower panel). mASC-1= murine endogenous ASC-1; hASC-1 = human ectopic ASC-1; hCelf1 = human ectopic Celf1. (D) Western blot analysis of pRb phosphorylation state in NT, Scbl and siTrip4 cells revealed a fast migrating band corresponding to the hypo-phosphorylated form of Rb (pRb, 110 kDa) and slower migrating bands corresponding to hyper-phosphorylated forms of Rb (ppRb, 116kDa) (left panel). Red ponceau (redP) staining of the membrane showed similar loading in each condition. In all conditions, the hyper-phosphorylated forms of Rb were predominant compared to the hypo-phosphorylated form as expected for cycling cells. Although variability precluded reaching statistical significance, quantification of the ratio ppRb/total pRb for each condition (N=4) showed an increase by nearly 50% of hyper-phosphorylated forms in siTrip4 cells (right panel).

Family Patient Gender	Family A III.2 F	Family B III.1, M III.2, F	Family C# III.7 M	Family D II.2 M	Family E II.4 M	Family F (Davignon et al, 2016) 1F, 3M
<b>TRIP4 Pathogenic variant</b>	c.141_142delAT (p.Tyr48fs*3) homozygous	c.534C>G (p.His178Gln) + c.1544_1547delACTG (p.Asp515fs*34)	c.1065delC (p.Ile356fs*6) homozygous	c.55_56insCT (p.Gln19fs*47) + c.1197delA (p.Ser399fs*12)	Homozygous deletion of exons 8 and 9	c.890G>A (p.Trp297*) homozygous
<b>First signs</b>	Hypotonia, DMM	DMM (gait acquisition) in both siblings Waddling gait and fatigability in III.2	NH, respiratory distress, feeding difficulties	NH, DMM	Difficulty running, poor sports performance (adolescence)	NH, Respiratory distress (n=3), feeding difficulties (n=3)
<b>Best motor performance</b>	Present age (9y): waddling gait, climb stairs, bipodal jump, starts to run	Present age (22y, III.1) and 16y (III.2): waddling gait, climb stairs	NA	Present age (35y): independent ambulation (short distances)	Adulthood: independent ambulation, climb stairs	Supported indoors ambulation in mildest patient until 11y
<b>Evolution of motor performance</b>	Improving	Stable	NA	Stable	Stable	WCB before adulthood
<b>Scoliosis</b>	Yes (early childhood)	Yes (early childhood)	No	Yes (early childhood) + Arthrodesis at 16y	No	Progressive scoliosis and arthrodesis in 3
<b>Rigid spine</b>	No	Yes in III.2	No	Yes	Yes	Yes (n=2)
<b>Respiratory involvement</b>	Respiratory infections since 7m. Nocturnal non-invasive ventilation since age 3y	Restrictive RF since childhood. Latest FVC 60% (III.1, 22y) and 52% (III.2, 18y). No assisted ventilation.	From birth. Neonatal respiratory distress needing tracheostomy and ventilation. Died from RF at 8m	Restrictive RF. Nocturnal non-invasive ventilation since 18y. Latest FVC 35% (35y)	Latest FVC 80% (63y). Obstructive sleep apnea syndrome treated by CPAP	From birth (n=3) and from 2y (n=1). Ventilation in the 1 <sup>st</sup> year of life in 3 and from 11y in the mildest
<b>Cardiac involvement</b>	No	No	No	No	DCM (LVEF 25%) in the 5 <sup>th</sup> decade	DCM in the 3 <sup>rd</sup> decade (n=1)
<b>Joint contractures</b>	Yes (Achilles)	No	No	Yes (elbows, achilles). Joint hyperlaxity LL	Yes (elbow, mild)	Yes (n=2); Hyperlaxity (n=4)
<b>Skin involvement</b>	No	No	Yes (hyperelasticity)	Yes (hyperelasticity, FH)	Yes (xerosis, FH)	Yes (hyperelasticity, xerosis, FH)
<b>Dysmorphic features</b>	Flat face, retrognathia	No	Flat face, prominent venous markings, tapering fingers	Elongated face, low-set ears, retrognathia. Flat thorax, pectus excavatum.	Flat face, retrognathia. Flat thorax, pectus excavatum.	Flat face (n=2), flat thorax (n=3), funnel thorax (n=1), pectus excavatum (n=2), valgus feet (n=2), high arched palate (n=1)
<b>Other features</b>	Underweight (<P3) Learning and writing difficulties	Right-eye keratoconus (III.1)  Underweight (<P4) (III.2)	Severe ophthalmoplegia	Underweight (<P3). Myopia	Mild ophthalmoparesis. Myopia	LL lipodystrophy (n=2), learning difficulties (n=2), language delay (n=1), testicular ectopia and delayed puberty (n=1)

**Table 1. Summarized clinical findings.** F: female; M: male; m: months; y: years; UK: unknown; NA: non applicable; NH: neonatal hypotonia; DMM: Delayed motor milestones; RF: respiratory failure; WCB: wheelchair-bound; CPAP: Continuous Positive Airway Pressure; DCM: Dilated cardiomyopathy; LVEF: Left ventricular ejection fraction; FH: follicular hyperkeratosis; LL: lower limbs; #Proband BOS1248-1 in The Manton Center for Orphan Disease Research database.

Patient	Age at biopsy	Muscle sampled	Major findings
AIII.2	4 years	Quadriceps	IN, FSV, type1 fiber predominance (95%) and hypotrophy, minimal endomysial fibrosis, whorled fibers, minicores
BIII.1	9 years	Quadriceps	Reported as normal
CIII.7	2 months	Quadriceps	IN, FSV, type1 fiber predominance and hypotrophy, endomysial fibrosis
DII.2	27 years	Biceps brachii	IN, FSV, type 1 fiber predominance (99%), minicores, rimmed sarcolemma
EII.4	56 years	2 Quadriceps biopsies	IN, FSV, type 1 fiber predominance, lobulated fibers; minicores in one biopsy; rods, cytoplasmic bodies and caps in a second biopsy

**Table 2. Main histological findings in skeletal muscle biopsies from five patients.** IN: internalized nuclei. FSV: abnormally increased fiber size variation.